

Task-Driven Semantic Quantization and Imitation Learning for Goal-Oriented Communications

Yu-Chieh Chao¹, Yubei Chen¹, Weiwei Wang¹, Achintha Wijesinghe¹, Suchinthaka Wanninayaka¹,
Songyang Zhang², *Member, IEEE*, and Zhi Ding¹, *Fellow, IEEE*

¹University of California at Davis, Davis, CA, USA

²University of Louisiana at Lafayette, Lafayette, LA, USA

Abstract—Semantic communication marks a new paradigm shift from bit-wise data transmission to semantic information delivery for the purpose of bandwidth reduction. To more effectively carry out specialized downstream tasks at the receiver end, it is crucial to define the most critical semantic message in the data based on the task or goal-oriented features. In this work, we propose a novel goal-oriented communication (GO-COM) framework, namely Goal-Oriented Semantic Variational Autoencoder (GOS-VAE), by focusing on the extraction of the semantics vital to the downstream tasks. Specifically, we adopt a Vector Quantized Variational Autoencoder (VQ-VAE) to compress media data at the transmitter side. Instead of targeting the pixel-wise image data reconstruction, we measure the quality-of-service at the receiver end based on a pre-defined task-incentivized model. Moreover, to capture the relevant semantic features in the data reconstruction, imitation learning is adopted to measure the data regeneration quality in terms of goal-oriented semantics. Our experimental results demonstrate the power of imitation learning in characterizing goal-oriented semantics and bandwidth efficiency of our proposed GOS-VAE.

Index Terms—Goal-oriented communications, imitation learning, semantic compression, generative learning.

I. INTRODUCTION

Next-generation wireless networks and Artificial Intelligence (AI) algorithms have found a wide range of data-intensive applications, including augmented and virtual reality [1], and autonomous driving [2], where low-latency data transport and high-accuracy decision-making play crucial roles. As these applications proliferate, the hunger for bandwidth and data rates continues to grow, straining the already scarce communication resources [3]. To achieve the bandwidth efficiency and ensure the data transmission quality, the concept of semantic communications has recently re-surfaced as an important paradigm, which aims at conveying the most critical semantic information rather than bit-wise packet transport [4].

Semantic communication systems commonly employ deep learning techniques for embedding representations and regenerating data. For example, DeepSC [5] focused on communicating the semantic meaning in text messages by utilizing a deep-learning transformer architecture. Beyond text communications, authors of [6] proposed a joint source and channel coding technique for wireless image transmission, using a Convolutional Neural Network (CNN) to directly map image pixels to channel input symbols. Another work (VQ-DeepSC [7]) presented a vector quantization semantic communication system to compress multi-scale semantic features through codebook quantization. The recent development of generative AI has further inspired other generative frameworks

for semantic communications. For example, in [8], a pre-trained Generative Adversarial Network (GAN) is utilized to reconstruct images at the receiver. Similarly, Generative Semantic Communication (GESCO) introduced in [9] utilizes a diffusion-based architecture for data generation based on segmentation maps. Nevertheless, these classic semantic communication frameworks continue to stress the visual quality of the reconstructed images. Future communication systems are expected to play an increasingly important part to serve automation, artificial intelligence, and other decision-making applications, instead of being a pipe to provide data to only human end-users. Thus, next-generation networks should also target the communication of task-driven semantic information essential for the accomplishment of major downstream tasks without involving human viewers. Efficient extraction of semantic features remains a key issue.

Recognizing key role of communication networks in AI-driven data applications, recent works have shifted towards task/goal-oriented semantic communication (GO-COM) systems [10]. Unlike classic semantic communications, these GO-COMs focus more on delivery of key semantic information for the specific downstream tasks at the receiver end. For this, [11] proposed a semantic image transmission system that allocates higher data rates to Regions of Interest (ROI) within images. However, ROIs can vary significantly across downstream tasks. The TasCom framework [12] addresses this by transmitting only task-specific features, using an Adaptive Coding Controller to prioritize those most relevant to AI performance. Similarly, VIS-SemCom [13] reduces redundancy by transmitting feature maps of key objects, such as vehicles and pedestrians, in scenes like autonomous driving. Despite these progresses, existing GO-COMs reconstruct data using pre-defined semantic features, which lack adaptivity and generalization. For instance, while trees may generally be considered non-essential in autonomous driving, an accidentally fallen tree branch obstructing the road would require immediate attention. Furthermore, onboard resources are often insufficient to manage multiple complex tasks with models containing billions of parameters [14]–[16]. Thus, critical challenges remain in advancing GO-COMs, particularly in achieving efficient semantic extraction and effective implementation.

To address the aforementioned challenges, this work introduces a novel GO-COM framework, namely Goal-Oriented Semantic Variational Autoencoder (GOS-VAE), integrating the Vector Quantized VAE (VQ-VAE) and imitation learning. We

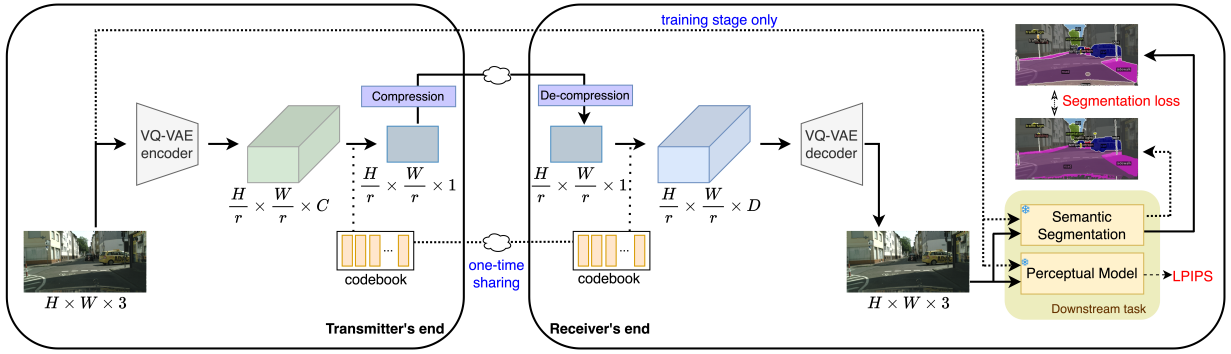


Fig. 1. The proposed Goal-Oriented Semantic Variational Autoencoder (GOS-VAE) framework for Semantic Communication: The snowflakes symbol denotes that fixed and pre-trained model parameters.

summarize our major contributions as follows:

- Taking autonomous driving as an exemplary application, we propose the novel GOS-VAE framework supported by a VQ-VAE backbone, which defines the goal-oriented “semantics” beneficial to the downstream task.
- To save computation, GOS-VAE places the decoder and computation-intensive downstream task model on a powerful back-end server while deploying a low-complexity encoder at the sender to improve efficiency.
- To preserve information vital to downstream tasks, our GOS-VAE adopts imitation learning capable of processing different tasks without manual labeling.
- Through flexible adjustment of network depth and codebook size, plus a customized shallow CNN structure, our proposed GOS-VAE achieves superior signal recovery performance at reduced bandwidth consumption.

II. METHOD

We begin by introducing the structure of GOS-VAE.

1) *Objective:* Our GOS-VAE focuses on application scenarios similar to autonomous driving, where edge devices such as autonomous vehicles or robots host limited computational power and is connected to back-end servers with powerful computing capacities. Particularly, we use image transmission for remote vehicle control as an exemplary application. While demonstrated on image transmission, our framework can be applied to a range of platforms supporting AI-driven tasks. Additionally, it emphasizes learning-based source embedding, adaptable to various channel models and communication protocols.

2) *Overall Structure:* The overall structure of our GOS-VAE is illustrated as Fig. 1. The transmitter features a lightweight encoder to embed the original images before transmitting a compressed representation to the receiver. The receiver reconstructs images for the accomplishment of its downstream tasks. Inspired by [7], a Vector Quantized-Variational AutoEncoder (VQ-VAE) [17] structure forms the backbone of the encoder-decoder model. Instead of focusing only on the visual quality of reconstructed images, we train a codebook to characterize semantic information for the downstream task. During training, we end-to-end optimize the entire framework through imitation learning with performance feedback from the downstream task. This work focuses on a single

task—semantic segmentation—leaving multi-task generalizations for future work. In the following sections, we introduce each functionality of our proposed GOS-VAE.

A. VQ-VAE Backbone

Our GOS-VAE uses VQ-VAE as encoder and decoder, deployed at the transmitter and the receiver, respectively. The transmitter input is an image $x \in \mathbb{R}^{H \times W \times 3}$, where H , W , and 3 denote the height, width, and the three RGB channels, respectively. The VQ-VAE encoder z_e compresses the image into a feature map $z_e(x) \in \mathbb{R}^{\frac{H}{r} \times \frac{W}{r} \times C}$, where r is the compression ratio affected by the multi-layer Convolutional Neural Network (CNN). Given the feature map, we use a codebook to further reduce transmission data payload. The channel dimension is reduced by a factor of C . Given a codebook $\mathbf{e} = \{e_i\}_{i=1}^K \in \mathbb{R}^{K \times D}$ of size K and codeword length D , a quantized map $z \in \mathbb{R}^{\frac{H}{r} \times \frac{W}{r}}$ based on a nearest-neighbor lookup can be found:

$$q(z_{ij} = k|x) = \begin{cases} 1 & \text{for } k = \arg \min_{\ell} \|z_e(x) - e_{\ell}\|_2, \\ 0 & \text{otherwise} \end{cases}. \quad (1)$$

Both the transmitter and the receiver should pre-store the learned codebook before real-time networking. After quantization, the transmitter sends the codeword index to the receiver which converts the codeword z back to its feature map, denoted as $z_q(x) \in \mathbb{R}^{\frac{H}{r} \times \frac{W}{r} \times D}$, which is calculated as

$$z_q(x)_{ij} = e_k, \quad \text{where } k = \arg \min_{\ell} \|z_e(x) - e_{\ell}\|_2. \quad (2)$$

The receiver forwards the feature map to its CNN decoder to recover the spatial dimension of the feature map and finally reconstruct the image $\hat{x} \in \mathbb{R}^{H \times W \times 3}$.

B. Post-Training Communication Showtime

During showtime, the transmitter only sends the codeword map z for each captured RGB image x to the receiver under compression ratio r . This compressed representation reduces bandwidth usage while preserving essential information. Furthermore, due to the skewed distribution of the learned codebook, the codeword map may be further compressed by entropy encoding. Our proposed framework trains the compression network VQ-VAE in an end-to-end manner in view of the downstream task to ensure that the codeword

map retains both good perceptual quality and the semantic information vital to downstream task performance. The details will be introduced in Section II-E.

C. Downstream Task

In this work, we use semantic segmentation as downstream task, which identifies the object category of each pixel. For this task, we adopt an open-source and pre-trained OneFormer [18] that unifies semantic, instance, and panoptic segmentation within a single model. Given an image $x \in \mathbb{R}^{H \times W \times 3}$, the pre-trained OneFormer F predicts the segmentation map as

$$S = \text{Softmax}(F(x)) \in \mathbb{R}^{H \times W \times m}, \quad (3)$$

where m is the number of object classes. The pre-trained OneFormer F is unchanged during the training phase. To leverage the information from the downstream tasks, reconstructed images are fed into the pre-trained networks to generate additional loss terms for deep training. Additional details are explained in the following sections.

D. Imitation Learning

Not relying on ground-truth segmentation labels, we apply imitation learning [19] to guide the learning process. The goal of GOS-VAE is to reconstruct an image that is at least semantically similar to the original. For example, if the segmentation map of the original image identifies a vehicle resembling an ambulance, the GOS-VAE system should reconstruct a vehicle with similar appearance. This ensures the preservation of critical semantic features, such as vehicle characteristics. Imitation learning could also eliminate the need for ground-truth labeling and manual intervention.

In our framework, the original image x first passes through the segmentation model F to generate the segmentation map $S \in \mathbb{R}^{H \times W \times m}$, which serves as the imitation target. The reconstruction from GOS-VAE \hat{x} is also given to the segmentation model F to define its segmentation map $\hat{S} \in \mathbb{R}^{H \times W \times m}$. The learning objective is to minimize the difference of distributions between the two segmentation maps.

E. Objective Function

For the VQ-VAE, the original loss function is designed for pixel-wise reconstruction, i.e., for $N = H \times W \times 3$,

$$L_v = \frac{1}{N} \sum_{i=1}^N (x_i - \hat{x}_i)^2 + \|\text{sg}[z_e(x)] - e\|_2^2 + \beta \|z_e(x) - \text{sg}[e]\|_2^2, \quad (4)$$

in which $\beta = 0.25$ is a constant, and ‘sg’ denotes the stop-gradient operator. The first term captures the Mean-Squared Error (MSE) between the two images and approximates the reconstruction loss $\log p(x|z_q(x))$. Since the gradient does not flow through the encoder due to the quantization step, the second and third terms of the loss are used to optimize the codebook and the encoder, respectively.

Since the proposed GOS-VAE focuses on the efficacy of downstream tasks according to the reconstruction, we replace the pixel-wise MSE with a task-incentivized loss. Specifically, given two predicted segmentation maps, where each pixel represents a probability distribution over object categories,

we compute the distribution distance using Jensen-Shannon Divergence (JSD), as described in Section II-D. Since OneFormer is a pre-trained and fixed segmentation model, its data distribution aligns with the training datasets. Without further perceptual constraint on the reconstruction, GOS-VAE would struggle to perform well on the downstream task. To address this issue, we incorporate the Learned Perceptual Image Patch Similarity (LPIPS) [20] as a perceptual regularization in the loss function, using a pre-trained VGG16 [21]. LPIPS compares two images by measuring the differences of their feature maps from the pre-trained VGG16. This term captures perceptual similarity, focusing on high-level semantic differences instead of pixel-wise changes. Finally, our objective function for the proposed GOS-VAE is

$$L_s = \text{LPIPS}(x, \hat{x}) + D_{JS}(S \parallel \hat{S}) + \|\text{sg}[z_e(x)] - e\|_2^2 + \beta \|z_e(x) - \text{sg}[e]\|_2^2, \quad (5)$$

where $D_{JS}(S \parallel \hat{S}) = \frac{1}{2} D_{KL}(S \parallel M) + \frac{1}{2} D_{KL}(\hat{S} \parallel M)$, $M = \frac{1}{2}(S + \hat{S})$, and D_{KL} denotes the Kullback-Leibler Divergence.

In this work, we provide several alternative training schemes for the proposed GOS-VAE. In the basic GOS-VAE, we train the model from scratch using the objective function L_s . For an upgrade model GOS-VAE*, we first pre-train a VQ-VAE using the original objective function L_v before fine-tuning based on the objective function L_s . We further tested new models, VQ-VAE[†] and the corresponding GOS-VAE[†], by replacing the CNN layers with Residual Blocks [22] and by increasing the codebook size. All these designs are studied, together with comprehensive discussions in Section III-A.

III. EXPERIMENTS & ANALYSES

A. Experimental Settings

1) *Dataset*: We test GOS-VAE using two datasets: Cityscapes [23] and ADE20K [24]. Cityscapes contains 2,975 training and 500 validation images, featuring high-resolution urban street scenes, annotated with 35 object categories for semantic segmentation. Among these object categories, 19 are considered after the pre-training setup of OneFormer [18]. ADE20K includes 20,100 training and 2,000 validation images with diverse indoor and outdoor scenes, covering 150 object categories for segmentation. For training, images are resized to 256×512 , with horizontal flipping augmentation.

2) *Baselines*: We compare with conventional JPEG, Autoencoder, VQ-VAE [17], VQ-GAN [25], and diffusion-based GESCO [9], using semantic segmentation as the downstream task. In addition, we also compare different alternative training schemes for our GOS-VAE including the basic GOS-VAE consisting of shallow CNN layers, GOS-VAE*, and GOS-VAE[†]. Specifically, in GOS-VAE[†], we replaced the shallow CNNs with Residual Blocks [22] and increased the codebook size from 512 to 12,000, to test the performance upper bound of Imitation Learning.

3) *Setups*: For the Cityscapes dataset, both VQ-VAE and GOS-VAE are trained for 500 epochs. GOS-VAE* and GOS-VAE[†] are initialized using the pre-trained VQ-VAE and VQ-VAE[†], respectively, before fine-tuning for 100 more epochs.

TABLE I
PERFORMANCE COMPARISONS ON THE CITYSCAPES SEMANTIC SEGMENTATION DATASET.

Models	Bandwidth (KB)	# params (M)	mIoU ↑ (%)	Accuracy ↑ (%)
JPEG	11.469	-	40.134	84.706
Autoencoder	12.833	0.13	12.924	48.418
VQ-GAN ($r=4$)	6.791	24.00	54.238	92.523
GESCO	14.526	674.71	<u>58.969</u>	95.351
VQ-VAE ($r=4$)	7.447	0.70	53.040	91.647
VQ-VAE [†] ($r=4$)	8.309	7.32	54.961	92.762
GOS-VAE ($r=4$)	8.321	0.70	57.342	93.176
GOS-VAE* ($r=4$)	8.385	0.70	57.612	93.209
GOS-VAE [†] ($r=4$)	10.092	7.32	61.318	<u>94.087</u>

TABLE II
PERFORMANCE COMPARISONS ON THE ADE20K SEMANTIC SEGMENTATION DATASET.

Models	# params (M)	mIoU (%) ↑	Accuracy (%) ↑
JPEG	-	32.111	77.474
Autoencoder	0.13	22.389	69.607
VQ-GAN ($r=4$)	24.00	38.738	80.674
GESCO	681.33	16.850	61.170
VQ-VAE ($r=4$)	0.70	38.366	80.333
VQ-VAE [†] ($r=4$)	7.32	38.612	80.887
GOS-VAE ($r=4$)	0.70	39.075	80.974
GOS-VAE* ($r=4$)	0.70	<u>39.128</u>	<u>81.019</u>
GOS-VAE [†] ($r=4$)	7.32	40.765	81.974

For both JPEG and Autoencoder, we adjust the compression ratio to obtain comparable transmission bandwidth or payload. The CNN-based Autoencoder is trained for 500 epochs. The VQ-GAN is trained for 272 epochs. GESCO is trained for 250,000 steps, equivalent to approximately 125 epochs, with a diffusion step of 100. Note that all 35 segmentation categories are utilized for GESCO training and testing to reproduce its performance without changing the proposed architecture.

For the ADE20K dataset, VQ-VAE and GOS-VAE are trained for 100 epochs, while GOS-VAE* and GOS-VAE[†] are initialized using the pre-trained VQ-VAE and VQ-VAE[†] weights and fine-tuned for an additional 40 epochs. The CNN-based Autoencoder is trained for 100 epochs. The VQ-GAN is trained for 32 epochs. GESCO is trained for 300,000 steps, equivalent to approximately 15 epochs, with a diffusion step of 100. Each of the proposed GOS-VAE alternatives is trained and tested using a single RTX 4090 GPU, while GESCO is trained on an A100 GPU.

B. Overall Reconstruction Quality

We first compare the overall quality of image reconstruction of different GO-COM frameworks. Particularly, we use the performance of downstream image segmentation as evaluation metrics, in terms of mean Intersection over Union (mIoU) and pixel-wise accuracy. We measure the bandwidth (payload) of the compressed data required by the receiver for image reconstruction. We compare the three different versions of our GOS-VAE against the Autoencoder, VQ-VAE, VQ-GAN, diffusion-based GESCO, together with the classic JPEG compression.

The experimental results are presented in Table I. Although performance can be easily improved by using more bandwidth at a compression ratio of $r = 2$, we focus on $r = 4$ here to prioritize bandwidth efficiency. More specifically, we set

all the methods with a similar payload for better illustration. From Table I, we first notice that VQ-VAE surpasses JPEG and Autoencoder in both improving performance and bandwidth reduction, owing to the use of codebook quantization. Moreover, we also notice that VQ-GAN achieves similar performance to VQ-VAE with more realistic image generation due to the discriminator. However, this addition also results in a significantly larger model size and longer training time. Next, by comparing GOS-VAE to VQ-VAE and VQ-GAN, we showcase the benefit of end-to-end learning in the compression network alongside the downstream task, as it preserves the semantic information critical to downstream task performance. Compared to the diffusion-based GESCO, we further observe that GOS-VAE achieves comparable performance while consuming significantly less bandwidth at a compression ratio $r = 4$. Note that GESCO requires the ground-truth semantic segmentation map and edge map to generate the corresponding image during both training and testing phases. Moreover, GESCO utilizes semantic segmentation maps with 35 object categories, utilizing more detailed information for image generation. In contrast, our method only uses 19 object categories, following the pre-trained OneFormer setup [18].

TABLE III
QUANTITATIVE COMPARISONS OF VISUAL QUALITY IN RECONSTRUCTED IMAGES USING THE CITYSCAPES DATASET.

Models	Cityscapes			ADE20K		
	MSE ↓	FID ↓	LPIS ↓	MSE ↓	FID ↓	LPIS ↓
VQ-GAN	0.006	20.212	0.130	0.012	12.383	0.177
GESCO	0.355	71.893	0.544	0.549	92.317	0.725
VQ-VAE [†]	0.002	25.273	0.172	0.004	15.466	<u>0.170</u>
GOS-VAE [†]	<u>0.005</u>	17.517	0.066	<u>0.008</u>	8.719	0.075

Next by comparing GOS-VAE[†] to GOS-VAE*, we see a notable improvement, particularly in mIoU. Additionally, GOS-VAE[†] outperforms GESCO in mIoU and achieves comparable pixel accuracy. This experiment highlights that even a slight increase in computation could lead to substantial gains in downstream task results without extra bandwidth. Notably, when comparing the number of trainable parameters, the proposed GOS-VAE[†] is about 92 times smaller than GESCO.

To evaluate the generalizability of our GOS-VAE, we present the results of semantic segmentation on the ADE20K dataset, whose results are presented in Table II. To ensure fair comparisons, we adjust the network structure to let each method maintain a similar bandwidth or payload. Our test results show that the proposed GOS-VAE[†] substantially outperforms the existing schemes in each of the evaluation metrics, a result consistent with that from test using Cityscapes. These results further validate the effectiveness of the proposed GOS-VAEs when processing a larger and more complex dataset. Furthermore, the number of trainable parameters in this case is about 93 times less than the diffusion-based GESCO.

Finally, in Semantic Communication, visual quality of reconstructed images is also essential; thus, we compare our proposed GOS-VAE[†] with three representative methods. As

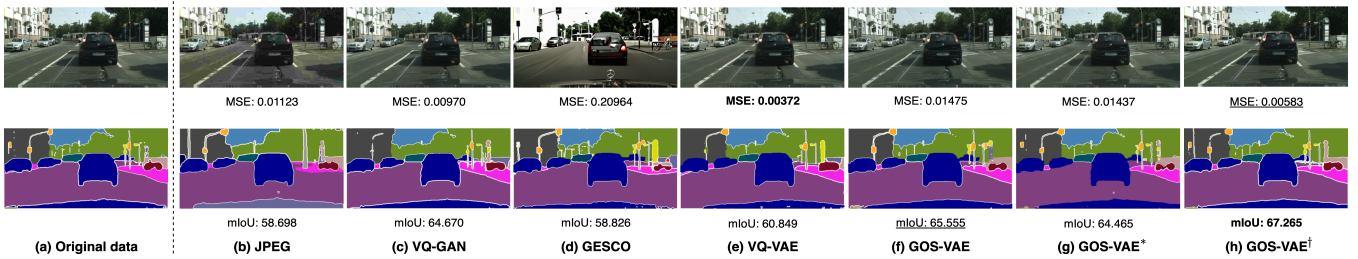


Fig. 2. Visualization Results of Different Methods on Cityscapes Dataset.

shown in Table III, GOS-VAE[†] achieves superior visual quality and closer alignment to the original image distribution, demonstrated by lower FID and LPIPS scores, rather than prioritizing pixel-wise accuracy as measured by MSE.

C. Visualization Results

In addition to numerical metrics, the visualization results of different approaches in image segmentation are presented in Fig. 2. From the results, we first notice that under limited transmission bandwidth, JPEG struggles to maintain good image quality and downstream task performance of the reconstructed images. Next, by comparing the proposed GOS-VAE[†] to all other methods, we underscore the benefit and power of goal-oriented semantic communication framework over communication systems designed for bit-wise recovery. More specifically, the image reconstructed by GOS-VAE[†] exhibits a high degree of visual consistency with the original one, even though it has a superficially higher pixel-wise Mean Squared Error (MSE) when compared against VQ-VAE. Moreover, in terms of the downstream segmentation task, GOS-VAE[†] successfully detects small while important objects, such as traffic signs and traffic lights, in its predicted segmentation map. However, VQ-GAN, VQ-VAE, and GESCO are not able to fully detect these important objects. Furthermore, the boundaries of many objects in the segmentation maps are not accurate. These results further demonstrate that GOS-VAE[†] is able to preserve the “semantic information” defined by the downstream task.

D. Ablation Study

1) *Performance with Different Objective Functions*: To illustrate the reasonability of our design of objective function for training our GOS-VAE as Eq. (5), we conduct an ablation study on different designs of loss function for GOS-VAE.

In the first setup, we use cross-entropy (CE) to measure the distribution similarity, denoted by GOS-VAE (CE), the loss can be characterized by

$$L_{sc} = CE(S || \hat{S}) + \|\text{sg}[z_e(x)] - e\|_2^2 + \beta \|z_e(x) - \text{sg}[e]\|_2^2. \quad (6)$$

We also apply the Kullback–Leibler divergence (KLD) for distribution comparison, which can be applied to both original VQ-VAE and GOS-VAE. For example, the VQ-VAE (KLD) can be trained based upon

$$L_{vk} = \frac{1}{N} \sum_{i=1}^N (x_i - \hat{x}_i)^2 + D_{KL}(S || \hat{S}) + \|\text{sg}[z_e(x)] - e\|_2^2 + \beta \|z_e(x) - \text{sg}[e]\|_2^2, \quad (7)$$

while GOS-VAE (KLD + LPIPS) has a similar objective function as Eq. (5) with the JSD replaced by the KLD.

For VQ-VAE (LPIPS), the pixel-wise Mean-Squared Error (MSE) is replaced with the LPIPS, while the downstream task loss is not included, calculated by

$$L_{vp} = \text{LPIPS}(x, \hat{x}) + \|\text{sg}[z_e(x)] - e\|_2^2 + \beta \|z_e(x) - \text{sg}[e]\|_2^2. \quad (8)$$

TABLE IV
ABLATION STUDY ON DESIGNING OBJECTIVE FUNCTION USING CITYSCAPES DATASET.

Models	mIoU (%) \uparrow	Accuracy (%) \uparrow
GOS-VAE (CE)	18.785	81.715
GOS-VAE (KLD)	42.792	89.028
VQ-VAE (KLD)	46.789	89.759
VQ-VAE (LPIPS)	54.933	92.479
GOS-VAE (KLD + LPIPS)	<u>56.949</u>	<u>93.166</u>
GOS-VAE (JSD + LPIPS)	57.342	93.176

As shown in Table IV, GOS-VAE (KLD+LPIPS) and GOS-VAE (JSD+LPIPS) consistently achieve the best performance, indicating the effectiveness of our proposed method on the downstream task. This can be attributed to the fact that the segmentation model, OneFormer, is pre-trained on the corresponding dataset, resulting in a data distribution that reflects images from the dataset. By utilizing LPIPS, data distribution of the reconstructed images aligns more closely with that of the OneFormer model, leading to improved performance. Compared to the CE-based method, KLD methods achieve better performance since KLD utilizes a distribution as the learning objective for each sample, providing more information than the one-hot label in Cross-Entropy.

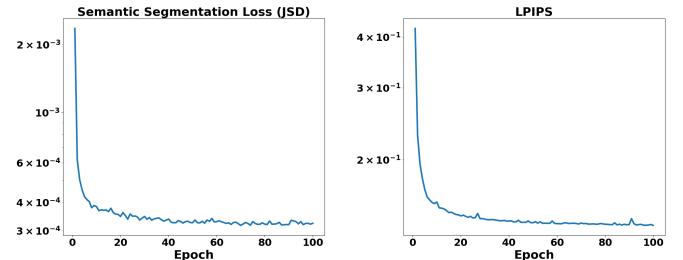


Fig. 3. Training curves of semantic segmentation loss (JSD) and LPIPS for GOS-VAE on the ADE20K dataset. The correlation of the two curves is 0.976.

We further analyze the relationship between semantic segmentation performance and LPIPS to further validate our conclusion. As shown in Fig. 3, the training curves for the two loss terms follow very similar trends with a correlation of 0.976. This indicates that managing the data distribution

shift is crucial for achieving optimal performance when using a pre-trained downstream task model to train an efficient compression network for GO-COM.

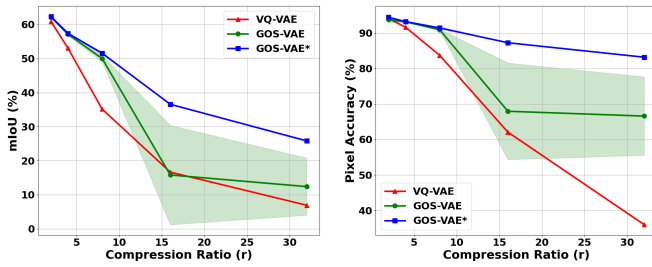


Fig. 4. Performance comparisons of models on the Cityscapes dataset under different compression ratios (r).

2) *Performance for Different Compression Ratios:* The tradeoff between compression ratio and downstream task performance is of critical concern for efficient data transmission. In this test, we compare the performance of semantic segmentation of reconstructed images from different methods at various compression ratios (r): 2, 4, 8, 16, and 32. From the results presented in Fig. 4, we observe that although GOS-VAE can achieve performance comparable to GOS-VAE*, its stability suffers at higher compression ratios. Moreover, GOS-VAE may fail to converge in some cases, with the worst-case mIoU dropping to as low as 5.462. The stability at higher compression ratios is the motivation for initializing GOS-VAE* with pre-trained VQ-VAE. On the other hand, GOS-VAE* consistently outperforms VQ-VAE across all compression ratios, establishing its superior stability and robustness, particularly in terms of pixel accuracy.

IV. CONCLUSION

In this work, we propose an innovative Goal-Oriented Semantic Variational Autoencoder (GOS-VAE) for task/goal-oriented communications, shifting the focus from visual quality or bit-wise recovery to conveying the task-driven semantic features. Particularly, the proposed GOS-VAE defines “semantic information” through end-to-end learning using a downstream task model. Leveraging the power of imitation learning, our proposed GOS-VAE is capable of preserving essential semantic information in the reconstructed images. Experimental results demonstrate that the proposed GOS-VAE framework delivers exceptional performance on the downstream task, surpassing previous methods while utilizing a low-complexity model architecture. Our future work plans to explore more advanced architectures for GO-COM, such as transformers and diffusion-based models, integrated with self-supervised learning.

REFERENCES

- [1] A. Hazarika and M. Rahmati, “Towards an evolved immersive experience: Exploring 5g-and beyond-enabled ultra-low-latency communications for augmented and virtual reality,” *Sensors*, vol. 23, no. 7, p. 3682, 2023.
- [2] S. Chen, J. Hu, Y. Shi, L. Zhao, and W. Li, “A vision of c-v2x: Technologies, field testing, and challenges with chinese development,” *IEEE Internet of Things Journal*, vol. 7, no. 5, pp. 3872–3881, 2020.

- [3] E. C. Strinati and S. Barbarossa, “6g networks: Beyond shannon towards semantic and goal-oriented communications,” *Computer Networks*, vol. 190, p. 107930, 2021.
- [4] X. Luo, H.-H. Chen, and Q. Guo, “Semantic communications: Overview, open issues, and future research directions,” *IEEE Wireless Communications*, vol. 29, no. 1, pp. 210–219, 2022.
- [5] H. Xie, Z. Qin, G. Y. Li, and B.-H. Juang, “Deep learning enabled semantic communication systems,” *IEEE Transactions on Signal Processing*, vol. 69, pp. 2663–2675, 2021.
- [6] E. Boursoulatzé, D. B. Kurka, and D. Gündüz, “Deep joint source-channel coding for wireless image transmission,” *IEEE Trans. Cognitive Comm. & Networking*, vol. 5, no. 3, pp. 567–579, 2019.
- [7] Q. Fu, H. Xie, Z. Qin, G. Slabaugh, and X. Tao, “Vector quantized semantic communication system,” *IEEE Wireless Communications Letters*, vol. 12, no. 6, pp. 982–986, 2023.
- [8] M. U. Lokumarambaga, V. S. S. Gowrisetty, H. Rezaei, T. Sivalingam, N. Rajatheva, and A. Fernando, “Wireless end-to-end image transmission system using semantic communications,” *IEEE Access*, vol. 11, pp. 37 149–37 163, 2023.
- [9] E. Grassucci, S. Barbarossa, and D. Comminiello, “Generative semantic communication: Diffusion models beyond bit recovery,” *arXiv preprint arXiv:2306.04321*, 2023.
- [10] X. Kang, B. Song, J. Guo, Z. Qin, and F. R. Yu, “Task-oriented image transmission for scene classification in unmanned aerial systems,” *IEEE Transactions on Communications*, vol. 70, no. 8, pp. 5181–5192, 2022.
- [11] J. Wu, C. Wu, Y. Lin, T. Yoshinaga, L. Zhong, X. Chen, and Y. Ji, “Semantic segmentation-based semantic communication system for image transmission,” *Digital Communications and Networks*, vol. 10, no. 3, pp. 519–527, 2024.
- [12] Y. Fu, W. Cheng, J. Wang, L. Yin, and W. Zhang, “Generative ai driven task-oriented adaptive semantic communications,” *arXiv preprint arXiv:2407.11354*, 2024.
- [13] J. Lv, H. Tong, Q. Pan, Z. Zhang, X. He, T. Luo, and C. Yin, “Importance-aware image segmentation-based semantic communication for autonomous driving,” *arXiv preprint arXiv:2401.10153*, 2024.
- [14] J. Achiam, S. Adler, S. Agarwal, L. Ahmad, I. Akkaya, F. L. Aleman, D. Almeida, J. Altenschmidt, S. Altman, S. Anadkat *et al.*, “Gpt-4 technical report,” *arXiv preprint arXiv:2303.08774*, 2023.
- [15] H. Touvron, T. Lavril, G. Izacard, X. Martinet, M.-A. Lachaux, T. Lacroix, B. Rozière, N. Goyal, E. Hambro, F. Azhar *et al.*, “Llama: Open and efficient foundation language models,” *arXiv preprint arXiv:2302.13971*, 2023.
- [16] H. Liu, C. Li, Q. Wu, and Y. J. Lee, “Visual instruction tuning,” *Advances in neural information processing systems*, vol. 36, 2024.
- [17] A. Van Den Oord, O. Vinyals *et al.*, “Neural discrete representation learning,” *Advances in neural information processing systems*, vol. 30, 2017.
- [18] J. Jain, J. Li, M. T. Chiu, A. Hassani, N. Orlov, and H. Shi, “One-former: One transformer to rule universal image segmentation,” in *Proc. IEEE/CVF Conf. on Comp. Vision & Pattern Recognition*, 2023, pp. 2989–2998.
- [19] D. Xu, Y. Chen, B. Ivanovic, and M. Pavone, “Bits: Bi-level imitation for traffic simulation,” in *2023 IEEE International Conference on Robotics and Automation (ICRA)*. IEEE, 2023, pp. 2929–2936.
- [20] R. Zhang, P. Isola, A. A. Efros, E. Shechtman, and O. Wang, “The unreasonable effectiveness of deep features as a perceptual metric,” in *Proc. IEEE Conf on Comp. Vision & Pattern Recog.*, 2018, pp. 586–595.
- [21] K. Simonyan and A. Zisserman, “Very deep convolutional networks for large-scale image recognition,” *arXiv preprint arXiv:1409.1556*, 2014.
- [22] K. He, X. Zhang, S. Ren, and J. Sun, “Deep residual learning for image recognition,” in *Proceedings of the IEEE conference on computer vision and pattern recognition*, 2016, pp. 770–778.
- [23] M. Cordts, M. Omran, S. Ramos, T. Rehfeld, M. Enzweiler, R. Benenson, U. Franke, S. Roth, and B. Schiele, “The cityscapes dataset for semantic urban scene understanding,” in *Proc. IEEE Conf. on Computer Vision & Pattern Recognition*, 2016, pp. 3213–3223.
- [24] B. Zhou, H. Zhao, X. Puig, T. Xiao, S. Fidler, A. Barriuso, and A. Torralba, “Semantic understanding of scenes through the ade20k dataset,” *Intl. J. of Computer Vision*, vol. 127, pp. 302–321, 2019.
- [25] P. Esser, R. Rombach, and B. Ommer, “Taming transformers for high-resolution image synthesis,” in *Proceedings of the IEEE/CVF conference on computer vision and pattern recognition*, 2021, pp. 12 873–12 883.